PCCP

PAPER

View Article Online
View Journal | View Issue

Published on 03 October 2014. Downloaded by Universitat Politecnica de Catalunya on 02/12/2014 12:16:35.

Cite this: *Phys. Chem. Chem. Phys.*, 2014, **16**, 24739

# Nanoantenna enhanced emission of light-harvesting complex 2: the role of resonance, polarization, and radiative and non-radiative rates†

Emilie Wientjes,[a] Jan Renger,[a] Alberto G. Curto,[ab] Richard Cogdell[c] and Niek F. van Hulst*[ad]

Received 14th August 2014,
Accepted 2nd October 2014

DOI: 10.1039/c4cp03636k

www.rsc.org/pccp

Nanoantennae show potential for photosynthesis research for two reasons; first by spatially confining light for experiments which require high spatial resolution, and second by enhancing the photon emission of single light-harvesting complexes. For effective use of nanoantennae a detailed understanding of the interaction between the nanoantenna and the light-harvesting complex is required. Here we report how the excitation and emission of multiple purple bacterial LH2s (light-harvesting complex 2) are controlled by single gold nanorod antennae. LH2 complexes were chemically attached to such antennae, and the antenna length was systematically varied to tune the resonance with respect to the LH2 absorption and emission. There are three main findings. (i) The polarization of the LH2 emission is fully controlled by the resonant nanoantenna. (ii) The largest fluorescence enhancement, of 23 times, is reached for excitation with light at $\lambda$ = 850 nm, polarized along the long antenna-axis of the resonant antenna. The excitation enhancement is found to be 6 times, while the emission efficiency is increased 3.6 times. (iii) The fluorescence lifetime of LH2 depends strongly on the antenna length, with shortest lifetimes of ~40 ps for the resonant antenna. The lifetime shortening arises from an 11 times resonant enhancement of the radiative rate, together with a 2–3 times increase of the non-radiative rate, compared to the off-resonant antenna. The observed length dependence of radiative and non-radiative rate enhancement is in good agreement with simulations. Overall this work gives a complete picture of how the excitation and emission of multi-pigment light-harvesting complexes are influenced by a dipole nanoantenna.

## Introduction

In the initial step of photosynthesis solar energy is absorbed by light-harvesting (LH) complexes, after which the excitation-energy is transferred rapidly and very efficiently to a reaction center where charge separation occurs.[1,2] To understand the amazingly high and robust transfer efficiency (>90%) several spectroscopic methods have been used to study photosynthetic systems at different levels. Particularly single-molecule fluorescence studies have given valuable information on the electronic properties of individual LH complexes, which are otherwise hidden in the ensemble average.[3,4] However, the low fluorescence quantum yield (QY) and poor photo-stability of LH complexes complicate such studies especially at physiologically relevant temperatures. To study the systems under nearly natural conditions one has to measure intact membranes. Combining spectroscopy with microcopy, in principle, allows spatial information of the heterogeneous membranes to be obtained.[5] Unfortunately, the size of the area excited by a strongly focused light beam (~300 nm diffraction limit) is orders of magnitudes larger than the size of a single light-harvesting complex which is in the range of 5–20 nm.[6,7]

Metal-nanoantennae are promising candidates in micro-spectroscopic photosynthesis research. Resonant excitation of the nanoantenna leads to the concentration of the electromagnetic fields into sub-diffraction limited volumes, as small as 10–50 nm in size.[8–10] Fluorophores placed in these localized "hot-spots" experience enhanced excitation rates. When the emission wavelength is resonant with the antenna, the high local density of optical states leads to enhancement of the radiative rate, which

[a] *ICFO – Institut de Ciencies Fotoniques, Mediterranean Technology Park, 08860 Castelldefels, Barcelona, Spain. E-mail: Niek.vanHulst@ICFO.eu*
[b] *Geballe Laboratory for Advanced Materials, Stanford University, Stanford, California 94305, USA*
[c] *Biomedical Research Building, Institute of Biomedical and Life Sciences, University of Glasgow, Glasgow, UK*
[d] *ICREA – Institució Catalana de Recerca i Estudis Avançats, 08010 Barcelona, Spain*

† Electronic supplementary information (ESI) available. See DOI: 10.1039/c4cp03636k

Published on 03 October 2014. Downloaded by Universitat Politecnica de Catalunya on 02/12/2014 12:16:35.

increases the fluorescence QY and shortens the fluorescence lifetime.[11] These enhancements can be used to increase the emission of single light-harvesting complexes up to 500 times.[12] Even over 1000-fold fluorescent enhancement has been reported for single dye molecules.[13,14] Moreover the spatially confined electromagnetic field potentially allows measurements on photosynthetic membranes with a very high spatial resolution of ~10 nm.[15]

To design an optimal nanoantenna for a specific experiment, it is important to understand the effect the antenna has on the excitation and emission of the fluorophore. On the emission side, it has been shown for quantum dots[16] and organic dyes[17,18] that the polarization is controlled by the resonant nanoantenna. Another effect is the modification of the emission spectrum, as the antenna most strongly enhances transitions resonant with the antenna.[19–23] Most importantly, nanoantennae are able to increase the fluorescence signal; the total enhancement is given by the product of excitation-enhancement and QY-enhancement. The intrinsic QY of a fluorophore ($QY_0$) is given by: $QY_0 = k_{r0}/(k_{r0} + k_{nr0})$, with $k_{r0}$ and $k_{nr0}$ being the intrinsic radiative and non-radiative decay rates. The nanoantenna enhances the radiative rate with the Purcell factor ($P$). However, as the fluorophore comes close to the metal surface a part of its emission is transferred to the metal and dissipated into heat; this occurs at the rate $k_{met}$.[24,25] The decay rates of the molecule in the presence of the antenna are thus: $k_r = P{\cdot}k_{r0}$, $k_{nr} = k_{nr0} + k_{met}$, and the $QY = k_r/(k_r + k_{nr})$. For a poor emitter with $QY_0 \ll 1$, the QY increases with the Purcell factor. However, for a good emitter with $QY_0$ close to unity, the QY will only decrease due to losses into the metal.[26] The enhancement of the radiative and non-radiative rate leads to a shortening of the fluorescence lifetime ($\tau$): $\tau = 1/(k_r + k_{nr})$. As the fluorophore spends less time in the excited state, the photostability will increase and thus a higher number of photons can be detected before irreversible photobleaching occurs.[27,28]

To date only a few studies on emission enhancement of light-harvesting complexes have been reported using chemically synthesized metal nanostructures such as silver island films,[29,30] gold,[31–33] and silver nanoparticles.[34] In most studies the individual contributions of excitation and QY changes to the total fluorescence enhancement have not been disentangled. In general, for simpler fluorophores, only a few experimental studies have investigated this[14,35,36] and quantified the specific contribution of the radiative and non-radiative decay rate enhancement.[25,37,38]

Here, we report the complete characterization (polarization, spectra and lifetime) of the enhanced emission of light-harvesting complex 2 (LH2) from purple photosynthetic bacteria when coupled to a gold nanorod antenna. Antennae of increasing lengths were used to investigate how the resonance wavelength affects these properties. Excitation at a wavelength non-resonant with the antenna allowed the relative QY enhancement as a function of antenna length to be quantified. Using this information and the fluorescent lifetimes we estimated the radiative and non-radiative rates independently. Next, by tuning the excitation wavelength in resonance with the antenna we determined the excitation enhancement as well. The combined effect of excitation and emission enhancement resulted in a total enhancement of 23 times. Our experiment and simulations give a detailed description of the interaction of the nanoantenna with LH2. The insight is important in order to be able to apply nanoantennae successfully and quantitatively in photosynthetic spectroscopy and microscopy.

## Results and discussion

### Light-harvesting complex 2 attached to an array of nanoantennae

LH2 from *Rhodopseudomonas acidophila* is a cylindrical chromophore–protein complex which coordinates 9 carotenoids, absorbing between 450 nm and 550 nm, 9 weakly excitonically interacting bacterioChlorophylls-*a* (bChls) absorbing at approximately 800 nm (B800 ring), and 18 strongly interacting bChls absorbing around 850–860 nm (B850 ring).[1,39] Light energy absorbed by the carotenoids and the B800 ring is transferred within one picosecond to the B850 ring,[40] from which emission occurs. The LH2 absorption and emission spectra are presented in Fig. 1a.

The resonance wavelength of a dipole antenna scales linearly with its length for light polarized parallel to the long antenna axis.[41] To match the resonance to the emission wavelength, gold nanorods (NRs) of different lengths were fabricated on a glass coverslip by electron-beam lithography, gold evaporation and lift-off. The height and width of the NRs were kept constant at 50 nm and 60 nm, respectively, while the lengths were increased in 10 nm steps from 110 nm to 220 nm. This allows the antenna resonance to be tuned with respect to the LH2 emission and excitation wavelengths (Fig. 1a and b). Two successive NR columns have the same rod lengths, but the orientation is with the long axis either parallel ($\parallel$) or perpendicular ($\perp$) to the polarization of the excitation light (Fig. 2a). The resonance wavelength of the $\perp$-NRs is around 620 nm for all the NR lengths (data not shown). The NR extinction (scattering + absorption) as a function of the NR lengths is plotted in Fig. 1b, for wavelengths corresponding to the excitation ($\lambda$ = 532 nm, 800 nm, 850 nm) and the LH2 emission ($\lambda \sim$ 870 nm). The large extinction at $\lambda$ = 800 nm and $\lambda$ = 850 nm for $\parallel$-NRs of certain lengths indicates that strong excitation enhancement is expected for these antennae. Such extinction does not occur for $\perp$-NR orientation or at $\lambda$ = 532 nm (Fig. 1b). The LH2 emission ($\lambda \sim$ 870 nm) overlaps well with the extinction spectra of the $L$ = 150–180 nm NRs; thus for these NRs emission enhancement is expected (independent of the wavelength or polarization of the excitation light).

LH2 was chemically attached to the gold NRs with a thiol self-assembled monolayer (SAM) of 16-amino-1-hexadecanethiol (Fig. 2a). The positively charged amino-groups (at pH 8) of the thiol SAM can interact with the negatively charged amino acids of the LH2 protein and as such link LH2 to the nanoantenna. The total distance between the LH2 emitter and the gold is the sum of the SAM thickness (2.3 nm[42]) and the distance between B850 and the SAM. Assuming that the LH2 cylinders lie flat on the SAM, as has been observed for various charged surfaces,[43] the B850 to

 This journal is © the Owner Societies 2014

Published on 03 October 2014. Downloaded by Universitat Politecnica de Catalunya on 02/12/2014 12:16:35.

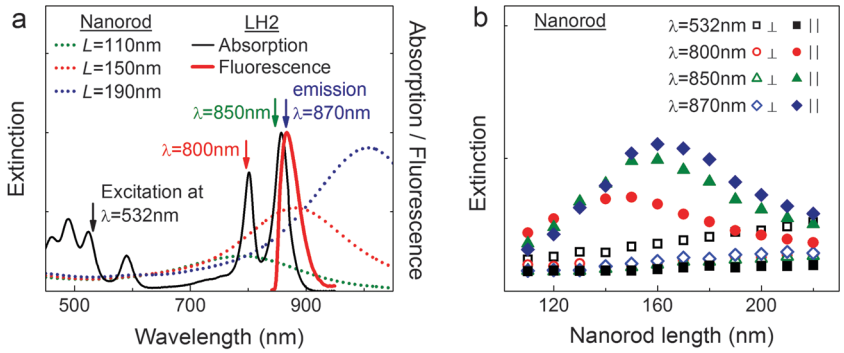


Fig. 1 Optical properties of gold nanorod antenna and light-harvesting complex 2 (LH2). (a) The absorption and emission spectra of LH2 in solution, and the extinction spectra of nanorods (NRs) of 3 different lengths. The NR spectra were measured on a large array in transmission with the polarization of the incident light parallel to the long-antenna axis. The different excitation wavelengths used in this study, and the LH2 emission wavelength ($\lambda \sim 870$ nm), are indicated. (b) Extinction of NRs for the three excitation wavelengths and the LH2 emission wavelength as a function of the NR length. The NRs are oriented with their long axis either perpendicular ($\perp$) or parallel ($\parallel$) with respect to the polarization of the incident light.

SAM distance is ~3.5 nm for LH2 from *Rhodopseudomonas acidophila*.[39,44] This gives a total spacing between the emitter and the surface of ~6 nm, while the distance to the B800 ring is ~1.5 nm less. In this arrangement strong enhancement of the radiative, non-radiative and excitation rates can be expected. In combination with the antenna array design this allows the enhancement effects to be studied as a function of both antenna lengths and orientation.

### Antenna modified polarization and spectrum of the LH2 emission

First we investigate the effect of the nanoantennae on the polarization of the LH2 emission. A confocal fluorescence image of a nanoantenna array was recorded for excitation with linearly polarized light at $\lambda = 532$ nm. Fig. 2b shows the Degree of Linear Polarization (DLP) of the fluorescence emission, defined as DLP = $(I_{\parallel} - I_{\perp})/(I_{\parallel} + I_{\perp})$ with $I_{\perp}$ and $I_{\parallel}$ the fluorescence intensity polarized perpendicular and parallel with respect to the excitation polarization (see Fig. 2a). The DLP changes between positive and negative, showing that the DLP is determined by the orientation of the long axis of the NRs in the array. The DLP is plotted against the NR length in Fig. 2c. The absolute values are highest for NRs in the range of $L$ = 140–180 nm, indicating that the LH2 emission is coupled most efficiently to these NRs. A maximum DLP of 0.74 ± 0.04 is reached for $L$ = 170 nm NRs, which is close to the theoretical maximum of 0.8 for the high numerical objective used in this work (NA = 1.46). The change of DLP to maximum values, both positive and negative, shows that the polarization of the LH2 emission can be fully controlled by the nanoantenna orientation.

A resonant antenna also modifies the emission spectrum of a fluorophore.[19–21] The presence of the antenna changes the local density of optical states, resulting in an enhanced probability of the transition of the lowest excited electronic state to specific ground state vibrations with the transition energy closest to the plasmon resonance energy. Emission spectra of single LH2–AuNR hybrid systems were recorded (Fig. 2d). The spectra shifted depending on the NR lengths. The strongest blue-shift was observed for $L$ = 130 nm NRs, while the emission spectrum was most red-shifted for $L$ = 190 nm NRs. Indeed the extinction maxima of the NRs peak at wavelengths shorter than the LH2 emission for $L$ = 130 nm NRs, while the maxima red-shift with increasing NR lengths. For NRs outside the $L$ = 130–190 nm range the spectral shaping is less pronounced, reflecting a weaker coupling between the LH2 emission and the antenna mode.

### Antenna enhanced LH2 emission

Next we focus on the fluorescence enhancement. First we excite at $\lambda$ = 532 nm, which is non-resonant for the NRs and excites $\parallel$-NRs of different lengths equally (Fig. 1b), and therefore only changes in the fluorescence QY will be observed. Confocal fluorescence images were recorded (Fig. 3a) and analyzed to extract the relative intensity for each NR length of the two orientations. The signal was first normalized to the antenna surface area available for LH2 binding, and next normalized to the signal for the NRs with $L$ = 220 nm, which is mostly out of resonance with the emission wavelength. The maximal enhancement is 3.6× for $L$ = 170 nm NRs (Fig. 3b). Slightly higher enhancement factors were found in the case of $\lambda$ = 532 nm excitation for $\perp$-NRs compared to $\parallel$-NRs (Fig. 3b), which can be attributed to a small contribution of enhanced excitation through the transversal mode.

Next we excite with $\lambda$ = 800 nm, which is expected to enhance the excitation of $\parallel$-NRs having their $\lambda/2$ plasmon resonance at this wavelength. A maximal enhancement of 15× is found for $\parallel$-NRs with length $L$ = 150 nm. This total enhancement arises from both excitation and emission enhancement. The contribution of the excitation enhancement can be separated by comparing resonant and non-resonant excitation, both as a function of the NR length, $L$. Thus we calculate the excitation enhancement as the ratio of total enhancement at 800 nm and 532 nm, for each length (Fig. 3d). The excitation enhancement reaches a maximum of 6× for the $L$ = 150 nm NR, in agreement with the largest extinction observed at this wavelength (Fig. 1b). No enhanced excitation is expected for $\perp$-NRs with $\lambda$ = 800 nm light, and therefore, they have the same spectrum as $\parallel$-NRs excited with $\lambda$ = 532 nm light. However, the enhancement for $\perp$-NRs at $\lambda$ = 800 nm around $L$ = 150 nm is somewhat higher

Published on 03 October 2014. Downloaded by Universitat Politecnica de Catalunya on 02/12/2014 12:16:35.

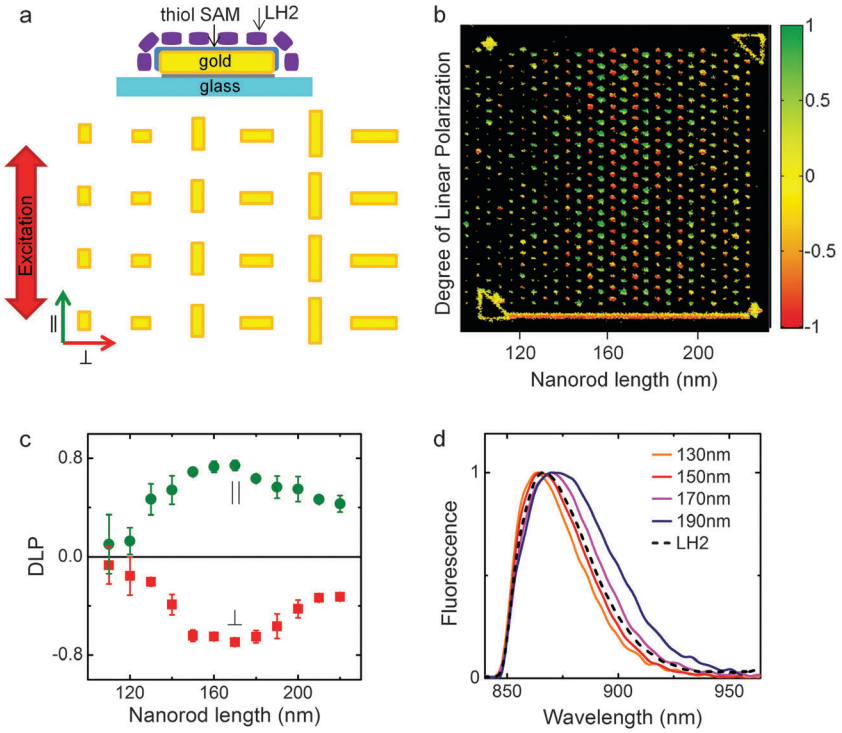


Fig. 2 Gold nanorods control the polarization of the LH2 emission. (a) Schematic representation of LH2 linked to the gold antenna by a self-assembled monolayer, and of the gold nanorod array with an increasing rod length and the rod oriented either ⊥ or ∥ with respect to the polarization of the excitation light. (b) The degree of linear polarization (DLP) of LH2-NR emission from an array of alternating ⊥ and ∥ NRs of increasing lengths, excitation was with $\lambda$ = 532 nm light. The polarization of the emitted light with respect to the excitation light is indicated by color, ⊥ is red and ∥ is green; black is shown when the total number of fluorescence counts was smaller than 6. (c) DLP as a function of the NR lengths. Average and standard deviations from 3 arrays are shown. For $L$ = 160–170 nm the emission is fully polarized along the antenna's long axis. (d) Fluorescence emission spectra of LH2-NRs are modified by the antenna resonance, with excitation at $\lambda$ = 800 nm.

than the non-resonant case (Fig. 3b). This can be attributed to the spatially inhomogeneous polarization of the excitation beam, which also contains perpendicular components in the focal spot of a high NA objective[45] and therefore to some extent oriented along the long antenna axis giving rise to enhanced excitation (see SI. 1, ESI†).

With excitation at $\lambda$ = 800 nm, the maximal enhanced excitation is reached for $L$ = 150 nm ∥-NRs, while the maximum of QY enhancement is found for $L$ = 170 nm NR. To fully benefit from the synergistic effect of both enhancement types the excitation needs to be tuned to a longer wavelength. Indeed shifting to light at $\lambda$ = 850 nm the excitation enhancement reached a maximum of 6× for $L$ = 170 nm ∥-NRs, giving a total enhancement of 23× (Fig. 3c and d). It should be noted that for $\lambda$ = 850 nm excitation a different long-pass filter ($\lambda$ = 885 nm) was used, which only transmits the long-wavelength part of the emission. This part is more enhanced by the longer NRs (Fig. 2d), giving rise to a somewhat higher apparent enhancement for these NRs.

### Resonant enhancement of the radiative and non-radiative decay rates

Radiative and non-radiative decay rates of a molecule in the proximity of a nanoantenna are altered due to the modified local density of optical states. The observed fluorescence enhancement is the result of the competition between both rates. Therefore, it is important to deduce the relative contribution of these two competing factors to the total fluorescence decay rate. Here we address this issue. All of the confocal fluorescence images were measured in the time-tagged time-resolved mode, which for every detected photon stores the photon arrival time relative to the corresponding laser excitation pulse and allows a fluorescence decay histogram to be constructed. Histograms were compiled for photons detected in the areas of the confocal image with NRs of the same lengths. Fig. 4a shows examples of histograms from a selection of LH2-NRs together with the instrument response function (45 ps at full-width half-maximum). The fluorescence lifetime was obtained by fitting the histograms with a sum of exponentials convoluted with the Instrument Response Function. A small contribution (typically 5%) of a slow decay component (0.5–0.9 ns) was needed to describe the data for each NR length. This component was ascribed to background fluorescence of uncoupled LH2s and therefore not taken into account further. One or two major components with (sub)100 ps lifetimes were needed to fit the decay histograms. The shortest (amplitude averaged) lifetime $\tau$ = 38 ps ($k_r + k_{nr}$ = 26 ns$^{-1}$) was found for $L$ = 160 nm LH2-NRs, indicating that the strongest resonant decay enhancement was reached for this antenna length. The longest lifetime $\tau$ = 125 ps ($k_r + k_{nr}$ = 8 ns$^{-1}$) was found for $L$ = 110 nm and $L$ = 220 nm NRs (Fig. 4b), which are both

 This journal is © the Owner Societies 2014

Published on 03 October 2014. Downloaded by Universitat Politecnica de Catalunya on 02/12/2014 12:16:35.

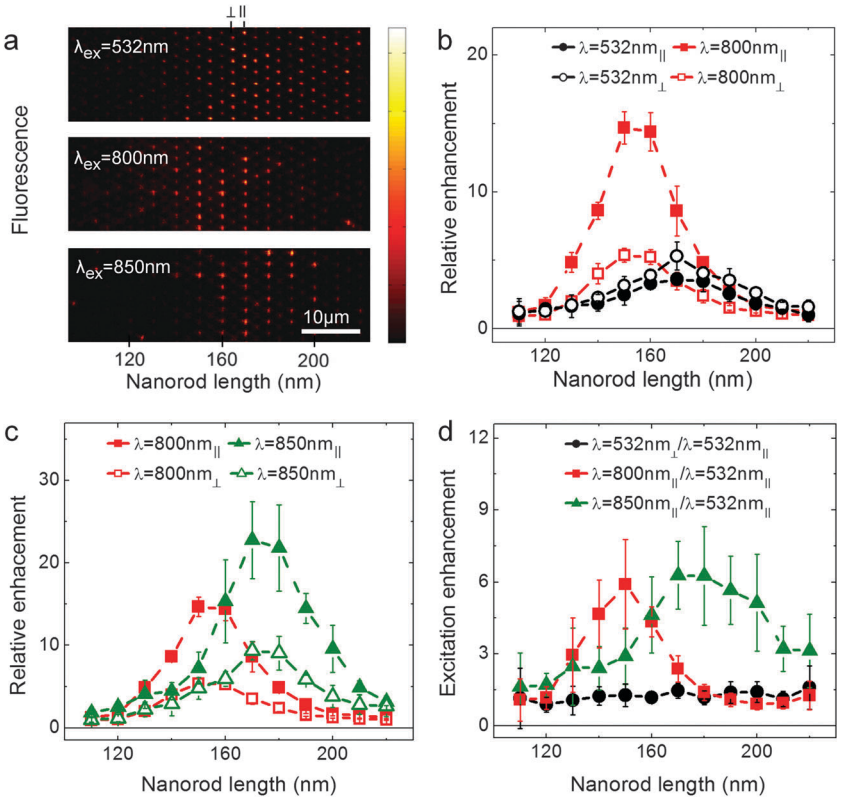


Fig. 3 Nanoantenna enhanced fluorescence of LH2 as a function of antenna lengths. (a) Confocal fluorescence images of a nanorod–LH2 hybrid array excited with $\lambda$ = 532 nm, $\lambda$ = 800 nm, and $\lambda$ = 850 nm; the NRs were oriented either parallel or perpendicular with respect to the polarization of the excitation light. Signals are normalized to the maximum intensity. (b, c) Enhancement of fluorescence intensity as a function of the NR length, relative to non-resonant nanorods of length $L$ = 220 nm nanorods ($\lambda$ = 532 nm, $\lambda$ = 800 nm) or $L$ = 110 nm ($\lambda$ = 850 nm). The strongest total enhancement is reached for $\lambda$ = 850 nm light polarized parallel to the long axis of the $L$ = 170 nm antenna. (d) Excitation intensity enhancement for the different wavelengths, obtained by dividing the total excitation wavelength dependent enhancement by the emission enhancement from the off-resonance excited $\lambda$ = 532 nm ||-NR. The dashed lines represent guidelines.

off-resonance with the LH2 emission (Fig. 1b). Nevertheless, 125 ps is far shorter than the lifetime of 1.1 ns measured for LH2 in solution (in agreement with literature values[46,47]). This lifetime reduction can partly be attributed to the short distance (6 nm) between the emitter and the antenna, allowing for quenching by non-resonant energy transfer to gold.[24,25] Also immobilization of the complex[47,48] and possibly singlet–singlet or singlet–triplet annihilation in LH2[49,50] can shorten the fluorescence lifetime. Finally, the $L$ = 110 nm and $L$ = 220 nm antennae are not completely out of resonance with the LH2 emission, as is particularly clear for the 220 nm NR for which the emission is still partly polarized along the antenna axis (Fig. 2c).

To be able to deduce the individual contributions of the radiative rate and the non-radiative rate to the fluorescence lifetime we need to know the quantum yield of the emission: QY = $k_r/(k_r + k_{nr}) = k_r \cdot \tau$. The QY of LH2-NRs of different lengths relative to $L$ = 220 nm is known from the measured emission enhancement spectrum (Fig. 3b, ||-NRs $\lambda$ = 532 nm). The radiative rate of the antenna enhanced emission is given by: $k_r = P \cdot k_{r0}$. The intrinsic LH2 radiative rate ($k_{r0}$) was assumed to be the same as in solution which is 0.1 $ns^{-1}$.[46] Thus the only unknown is the Purcell factor for the $L$ = 220 nm antenna. As a first approach we have assumed several reasonable values for $P$: 1, 6 and 12. With these $P$ values both $k_r$ and $k_{nr}$, as a function of the antenna length, were determined from the experimental lifetime and enhancement data (Fig. 5a). The $k_r$ is enhanced 11 times for $L$ = 160 nm NRs compared to $L$ = 220 nm, independent of the assumed Purcell factor. Importantly, $k_{nr}$ is also resonantly enhanced by a factor of 2 to 3. This non-radiative rate enhancement can be explained by the increased spectral overlap between the fluorescence of the emitter and the absorption of the metal, leading to more efficient energy transfer to the gold.[37,38]

To explore these findings further we performed finite-difference time-domain simulations[26] of the antenna-emitter system (FDTD Solutions, Lumerical). The LH2 with its 27 BChl is modeled as a single point dipole source. This simplification is justified by considering that the dipole which is mostly enhanced also contributes most to the fluorescence signal.[12] The dipole source was positioned at a distance of 6 nm from the end of the antenna and oriented longitudinally with respect to the antenna axis. The radiative rate enhancement (Purcell factor) was calculated as a function of wavelength for the NRs of different lengths. The values obtained at the LH2 emission wavelength ($\lambda$ = 870 nm) are plotted in Fig. 5b. The QY of the antenna ($QY_{ant}$), which is the fraction of energy radiated into the far-field, is also shown. Two different positions for the dipole source at the end of the

Published on 03 October 2014. Downloaded by Universitat Politecnica de Catalunya on 02/12/2014 12:16:35.

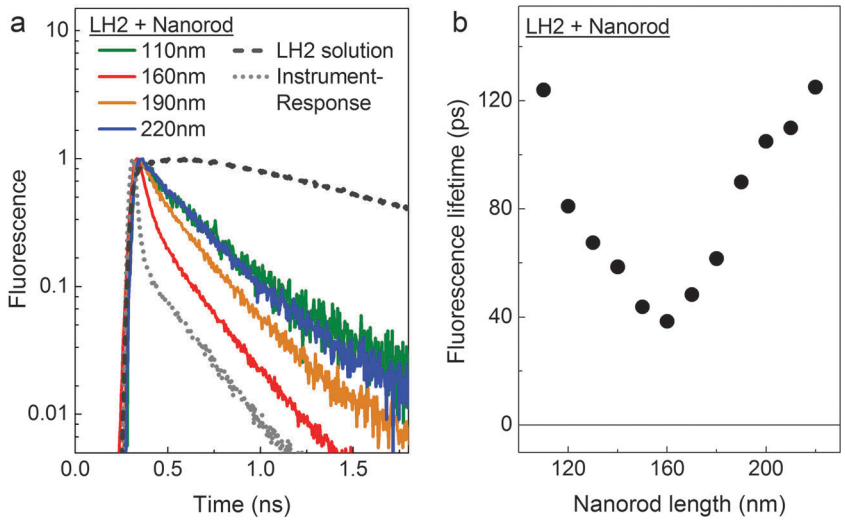


Fig. 4 Resonant enhancement of the LH2 fluorescence decay. (a) Fluorescence decay traces of LH2 coupled with nanorod (NR) antennae of different lengths, LH2 in solution, and the Instrument Response Function. (b) Fluorescence lifetime of LH2-NR as a function of the NR lengths. The fluorescence lifetime is strongly decreased for the resonant antenna.

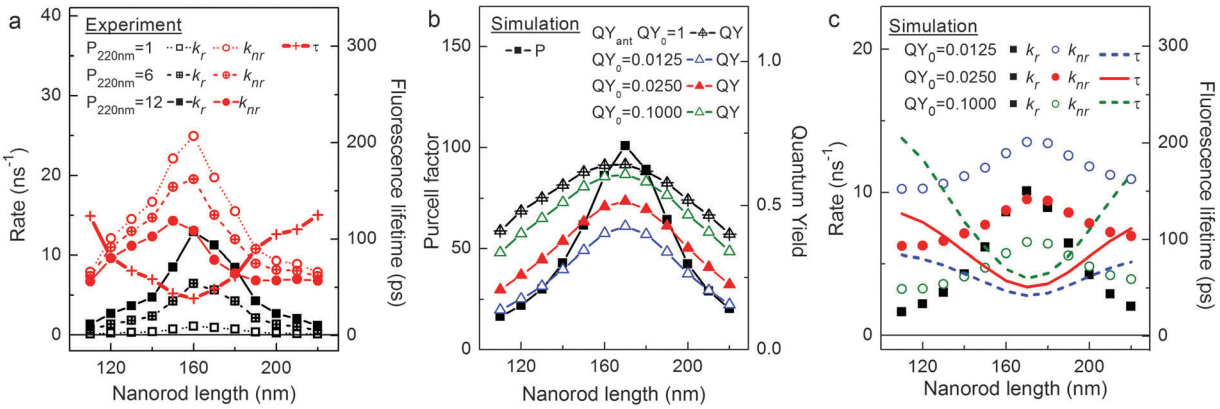


Fig. 5 Modification of the radiative and non-radiative emission rates as a function of the nanoantenna length – experiment and FDTD simulation. (a) Radiative and non-radiative rates of the LH2-NR emission as a function of the nanorod length, calculated from the measured fluorescence lifetime and fluorescence QY enhancement (Fig. 3a) relative to NR $L$ = 220 nm assuming a Purcell factor of 1, 6, or 12. (b) Fraction of energy radiated into the far-field from a dipole source (emitting at $\lambda$ = 870 nm) positioned at 6 nm distance from the end of the antenna and oriented longitudinally with respect to it. The intrinsic quantum yield ($QY_0$) of the dipole emitter was assumed to be 1.0 (showing the QY of the antenna), 0.0125, 0.025 or 0.1. (c) Simulation of the radiative rate, non-radiative rate and fluorescence lifetime of a dipole source, positioned as in (b) with respect to the nanorod. Both the radiative rate and the non-radiative rate are resonantly enhanced.

antenna were also modeled (see SI. 2, ESI†). Both positions showed a comparable NR length dependent change of the Purcell factor, albeit with lower values. The $QY_{ant}$ was almost unaffected, meaning that the non-radiative losses were decreased equally strongly as the radiative rate. The total QY of the coupled antenna-emitter system was calculated based on $QY_{ant}$, $P$ and the intrinsic QY of the emitter ($QY_0$) according to:[26]

$$QY = \frac{QY_0}{(1 - QY_0)/P + QY_0/QY_{ant}}$$

The $QY_0$ for LH2 in solution is 0.1;[46] however the immobilization process itself probably led to a decrease of the quantum yield, therefore lower values were also used for the calculation (Fig. 5b). These values were used to calculate the radiative rate, non-radiative rate and the fluorescence lifetime of the coupled system (Fig. 5c). With $QY_0$ = 0.025 the measured fluorescence lifetimes were adequately reproduced. The simulation shows that the radiative rate is strongly NR length dependent and that the non-radiative loss is resonantly enhanced, in agreement with the experimental observations (Fig. 5a). The resonant non-radiative rate enhancement is often overlooked, but it decreases both the fluorescence lifetime and the fluorescence QY of the coupled system and is therefore an important factor to take into account.

## Conclusion

The use of metallic nanoantennae is gaining ground in fundamental science and enables novel applications. Indeed the

 This journal is © the Owner Societies 2014

Published on 03 October 2014. Downloaded by Universitat Politecnica de Catalunya on 02/12/2014 12:16:35.

interaction of nanoantennae with single photon emitters has already been investigated in great depth. However, if we want to use nanoantennae for photosynthesis research it is crucial to understand how nanoantennae influence the emission properties of light-harvesting complexes that coordinate multiple excitonically interacting pigments. In this work we have studied the interaction between dipole nanorod antennae and light-harvesting complex 2 (LH2) from purple bacteria. The polarization of the LH2 emission was fully controlled by the resonant antenna. The fluorescence intensity was enhanced 23 times by a combination of both excitation and emission enhancement. Experimental data and simulations show that the radiative rate is strongly enhanced by the resonant antenna, however also that the non-radiative rate is increased. The combination of both processes leads to a strong reduction of the fluorescence lifetime. The interplay of all these effects needs to be carefully considered when designing an experiment for photosynthesis research. Most importantly it opens up ways to explore photosynthetic complexes with much higher sensitivity on a localized scale under natural conditions.

## Materials and methods

### Sample preparation

Light-harvesting complex 2 (LH2) was purified from *Rhodopseudomonas acidophila* (strain 10 050).[31] Gold nanorods (NRs) of different lengths were fabricated on a glass coverslip with a 50 nm Au layer and a 1 nm titanium adhesion layer by negative-tone electron-beam lithography in combination with reactive-ion etching. The NRs were covered with a SAM of 16-amino-1-hexadecanethiol (Dojindo EU GmbH) by placing them overnight in a 1 mM solution in ethanol; unbound molecules were removed by rinsing with ethanol and 1 minute of sonication in ethanol. LH2 was diluted to an $OD_{860\,nm}$ of 0.5 $cm^{-1}$ in buffer (0.1% LDAO, 20 mM Tris, pH 8.0) and incubated with the SAM covered gold NRs for 2 minutes. Free LH2 complexes were removed by gently washing with the buffer.

### Time-resolved confocal microscopy

Microscopy was performed using a commercial time-resolved confocal microscope (Micro Time 200, PicoQuant, Germany). The excitation was with linearly polarized light at $\lambda$ = 800 nm or $\lambda$ = 850 nm (titanium–sapphire pulsed laser, coherent) or $\lambda$ = 532 nm (PicoQuant diode laser), with a repetition rate of 76 MHz or 50 MHz, respectively. A high numerical aperture (1.46, 100×, Zeiss) oil immersion objective mounted on an inverted microscope (Olympus) was used for both excitation and collection. The fluorescence light was separated from the excitation light using a dichroic mirror and long pass filters ($\lambda$ = 835 nm + 850 nm) and detected on a single photon avalanche diode (PDM, Micro Photon Devices). Images were recorded by raster scanning the objective in 100 or 150 nm steps over the sample.

### Analysis of confocal images

The fluorescence counts of the confocal images were integrated in the *y*-direction to obtain the total fluorescence counts of the NR–LH2 hybrids of a specific length and orientation. The small level of background fluorescence was subtracted. The fluorescence counts from each NR lengths were divided by the exposed surface area, to correct for the different amount of LH2 complexes which can bind to gold. The fluorescence level was normalized to the $L$ = 220 nm NRs (parallel excitation for $\lambda$ = 532 nm, and perpendicular excitation for $\lambda$ = 800 nm and $\lambda$ = 850 nm excitation).

## Conflicts of interest

The authors declare no competing financial interests.

## Acknowledgements

We thank Lukasz Piatkowski for the spectral measurements. This research was funded by the European Commission (ERC Advanced Grant 247330-Nano Antennas), Fundació CELLEX (Barcelona) and Plan Nacional project FIS2012-35527. R.C. thanks the Biotechnology and Biological Sciences Research Council (BBSRC) for financial support. E.W. acknowledges financial support from the Marie-Curie International Fellowship COFUND and ICFOnest program.

## References

1 R. J. Cogdell, A. Gall and J. Köhler, *Q. Rev. Biophys.*, 2006, **39**, 227–324.
2 R. Croce and H. van Amerongen, *Photosynth. Res.*, 2013, **116**, 153–166.
3 R. Hildner, D. Brinks, J. B. Nieder, R. J. Cogdell and N. F. van Hulst, *Science*, 2013, **340**, 1448–1451.
4 A. M. van Oijen, M. Ketelaars, J. Kohler, T. J. Aartsma and J. Schmidt, *Science*, 1999, **285**, 400–402.
5 T. K. Goral, M. P. Johnson, A. P. Brain, H. Kirchhoff, A. V. Ruban and C. W. Mullineaux, *Plant J.*, 2010, **62**, 948–959.
6 X. W. Pan, M. Li, T. Wan, L. F. Wang, C. J. Jia, Z. Q. Hou, X. L. Zhao, J. P. Zhang and W. R. Chang, *Nat. Struct. Mol. Biol.*, 2011, **18**, U309–U394.
7 A. Ben-Shem, F. Frolow and N. Nelson, *Nature*, 2003, **426**, 630–635.
8 D. P. Fromm, A. Sundaramurthy, P. J. Schuck, G. Kino and W. E. Moerner, *Nano Lett.*, 2004, **4**, 957–961.
9 P. Mühlschlegel, H. J. Eisler, O. J. Martin, B. Hecht and D. W. Pohl, *Science*, 2005, **308**, 1607–1609.
10 T. H. Taminiau, R. J. Moerland, F. B. Segerink, L. Kuipers and N. F. van Hulst, *Nano Lett.*, 2007, **7**, 28–33.
11 J. N. Farahani, D. W. Pohl, H. J. Eisler and B. Hecht, *Phys. Rev. Lett.*, 2005, **95**, 017402.
12 E. Wientjes, J. Renger, A. G. Curto, R. Cogdell and N. F. van Hulst, *Nat. Commun.*, 2014, **5**, 4236.
13 H. Yuan, S. Khatua, P. Zijlstra, M. Yorulmaz and M. Orrit, *Angew. Chem., Int. Ed.*, 2013, **52**, 1217–1221.

Published on 03 October 2014. Downloaded by Universitat Politecnica de Catalunya on 02/12/2014 12:16:35.

14 A. Kinkhabwala, Z. F. Yu, S. H. Fan, Y. Avlasevich, K. Mullen and W. E. Moerner, *Nat. Photonics*, 2009, **3**, 654–657.
15 M. Mivelle, T. S. van Zanten, L. Neumann, N. F. van Hulst and M. F. Garcia-Parajo, *Nano Lett.*, 2012, **12**, 5972–5978.
16 A. G. Curto, T. H. Taminiau, G. Volpe, M. P. Kreuzer, R. Quidant and N. F. van Hulst, *Nat. Commun.*, 2013, **4**, 1750.
17 T. H. Taminiau, F. D. Stefani, F. B. Segerink and N. F. Van Hulst, *Nat. Photonics*, 2008, **2**, 234–237.
18 T. Ming, L. Zhao, H. Chen, K. C. Woo, J. Wang and H. Q. Lin, *Nano Lett.*, 2011, **11**, 2296–2303.
19 T. Ming, L. Zhao, Z. Yang, H. Chen, L. Sun, J. Wang and C. Yan, *Nano Lett.*, 2009, **9**, 3896–3903.
20 M. Ringler, A. Schwemer, M. Wunderlich, A. Nichtl, K. Kurzinger, T. A. Klar and J. Feldmann, *Phys. Rev. Lett.*, 2008, **100**, 203002.
21 E. C. Le Ru, P. G. Etchegoin, J. Grand, N. Felidj, J. Aubard and G. Levi, *J. Phys. Chem. C*, 2007, **111**, 16076–16079.
22 K. Tanaka, E. Plum, J. Y. Ou, T. Uchino and N. I. Zheludev, *Phys. Rev. Lett.*, 2010, **105**, 227403.
23 L. Zhao, T. Ming, H. J. Chen, Y. Liang and J. F. Wang, *Nanoscale*, 2011, **3**, 3849–3859.
24 P. Anger, P. Bharadwaj and L. Novotny, *Phys. Rev. Lett.*, 2006, **96**, 113002.
25 S. Kühn, U. Håkanson, L. Rogobete and V. Sandoghdar, *Phys. Rev. Lett.*, 2006, **97**, 1–4.
26 A. Mohammadi, V. Sandoghdar and M. Agio, *New J. Phys.*, 2008, **10**, 105015.
27 J. V. Pellegrotti, G. P. Acuna, A. Puchkova, P. Holzmeister, A. Gietl, B. Lalkens, F. D. Stefani and P. Tinnefeld, *Nano Lett.*, 2014, **14**, 2831–2836.
28 H. Cang, Y. Liu, Y. Wang, X. Yin and X. Zhang, *Nano Lett.*, 2013, **13**, 5949–5953.
29 M. H. Chowdhury, K. Ray, K. Aslan, J. R. Lakowicz and C. D. Geddes, *J. Phys. Chem. C*, 2007, **111**, 18856–18863.
30 J. B. Nieder, R. Bittl and M. Brecht, *Angew. Chem., Int. Ed.*, 2010, **49**, 10217–10220.
31 S. R. Beyer, S. Ullrich, S. Kudera, A. T. Gardiner, R. J. Cogdell and J. Kohler, *Nano Lett.*, 2011, **11**, 4897–4901.
32 L. Bujak, N. Czechowski, D. Piatkowski, R. Litvin, S. Mackowski, T. H. P. Brotosudarmo, R. J. Cogdell, S. Pichler and W. Heiss, *Appl. Phys. Lett.*, 2011, **99**, 173701.
33 L. Bujak, M. Olejnik, T. H. Brotosudarmo, M. K. Schmidt, N. Czechowski, D. Piatkowski, J. Aizpurua, R. J. Cogdell, W. Heiss and S. Mackowski, *Phys. Chem. Chem. Phys.*, 2014, **16**, 9015–9022.
34 I. Kim, S. L. Bender, J. Hranisavljevic, L. M. Utschig, L. B. Huang, G. P. Wiederrecht and D. M. Tiede, *Nano Lett.*, 2011, **11**, 3091–3098.
35 E. Bermúdez Ureña, M. P. Kreuzer, S. Itzhakov, H. Rigneault, R. Quidant, D. Oron and J. Wenger, *Adv. Mater.*, 2012, **24**, Op314–Op320.
36 H. Aouani, O. Mahboub, N. Bonod, E. Devaux, E. Popov, H. Rigneault, T. W. Ebbesen and J. Wenger, *Nano Lett.*, 2011, **11**, 637–644.
37 K. Munechika, Y. Chen, A. F. Tillack, A. P. Kulkarni, I. J. Plante, A. M. Munro and D. S. Ginger, *Nano Lett.*, 2010, **10**, 2598–2603.
38 O. L. Muskens, V. Giannini, J. A. Sanchez-Gil and J. G. Rivas, *Nano Lett.*, 2007, **7**, 2871–2875.
39 G. McDermott, S. M. Prince, A. A. Freer, A. M. Hawthornthwaite-Lawless, M. Z. Papiz, R. J. Cogdell and N. W. Isaacs, *Nature*, 1995, **374**, 517–521.
40 V. Sundstrom, T. Pullerits and R. van Grondelle, *J. Phys. Chem. B*, 1999, **103**, 2327–2346.
41 G. W. Bryant, F. J. G. De Abajo and J. Aizpurua, *Nano Lett.*, 2008, **8**, 631–636.
42 M. D. Porter, T. B. Bright, D. L. Allara and C. E. D. Chidsey, *J. Am. Chem. Soc.*, 1987, **109**, 3559–3568.
43 M. A. Bopp, Y. W. Jia, L. Q. Li, R. J. Cogdell and R. M. Hochstrasser, *Proc. Natl. Acad. Sci. U. S. A.*, 1997, **94**, 10630–10635.
44 D. E. Chandler, J. Hsin, C. B. Harrison, J. Gumbart and K. Schulten, *Biophys. J.*, 2008, **95**, 2822–2836.
45 L. Novotny and B. Hecht, *Principles of Nano-Optics*, Cambridge University Press, Cambridge, 2012.
46 R. Monshouwer, M. Abrahamsson, F. vanMourik and R. vanGrondelle, *J. Phys. Chem. B*, 1997, **101**, 7241–7248.
47 H. Ikemoto, S. Tubasum, T. Pullerits, J. Ulstrup and Q. J. Chi, *J. Phys. Chem. C*, 2013, **117**, 2868–2878.
48 X. H. Chen, L. Zhang, Y. X. Weng, L. C. Du, M. P. Ye, G. Z. Yang, R. Fujii, F. S. Rondonuwu, Y. Koyama, Y. S. Wu and J. P. Zhang, *Biophys. J.*, 2005, **88**, 4262–4273.
49 T. J. Pflock, S. Oellerich, J. Southall, R. J. Cogdell, G. M. Ullmann and J. Kohler, *J. Phys. Chem. B*, 2011, **115**, 8813–8820.
50 T. J. Pflock, S. Oellerich, L. Krapf, J. Southall, R. J. Cogdell, G. M. Ullmann and J. Kohler, *J. Phys. Chem. B*, 2011, **115**, 8821–8831.

 This journal is © the Owner Societies 2014